ACS OMEGA

Open Access

http://pubs.acs.org/journal/acsodf

Article

Selective SERS Detection of TATB Explosives Based on Hydroxy-Terminal Nanodiamond-Multilayer Graphene Substrate

Lin Jiang, Huiqiang Liu,* Bing Wang, Wen Zhang, Jian Wang, and Ying Xiong*

Cite This: *ACS Omega* 2024, 9, 22166−22174

Read Online

ACCESS | Metrics & More | Article Recommendations

ABSTRACT: Selective surface-enhanced Raman scattering (SERS) detection of target explosives with good reproducibility is very important for monitoring soldiers' health and ecological environment. Here, the specific charge transfer pathway was constructed between a stable nanodiamond-multilayer graphene (MGD) film substrate and the target explosives. Two-step wet chemical oxidation methods of H_2O_2 (30%) and HNO_3 (65%) solutions were used to regulate the terminal structure of MGD films. The experimental results showed that the hydroxyl (−OH) functional groups are successfully modified on the surface of MGD thin films, and the MGD−OH substrates having good selectivity for 1,3,5-triamino-2,4,6-trinitrobenzene (TATB) explosive in mixed solutions of the TATB, 2,2-dinitroethene-1,1-diamine, 2,4,6-trinitrotoluene, and 1,3,5-trinitroperhydro-1,3,5-triazine explosives compared with MGD substrates were demonstrated. Finally, first-principles density functional theory simulations revealed that the SERS enhancement of the MGD−OH substrate is mainly attributed to the transferred electrons between the $-NO_2$ groups of TATB and the −OH groups of the MGD−OH substrate.

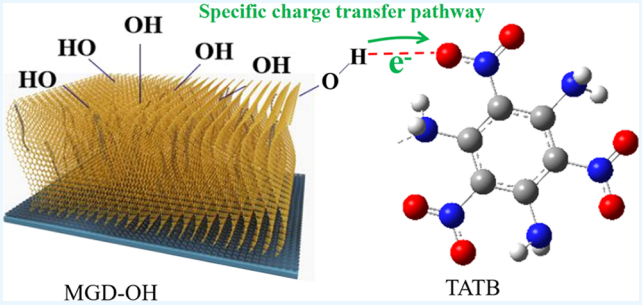

1. INTRODUCTION

As an indispensable destructive energy in various weapon systems, explosives are important strategic materials all around the world. Generally, explosives are used in military activities, and the residues of explosives after the explosion will cause serious pollution of air, water, and soil.[1,2] Long-term exposure of soldiers to explosive residues can cause serious harm to the body; especially, accidental drinking of drinking water contaminated with explosives can cause severe symptoms such as convulsions, vomiting, coma, etc.[3] Therefore, it is essential to identify the target explosives in a complex environment.

Surface-enhanced Raman scattering (SERS) technology has occupied an important position in the nondestructive selective detection of explosive molecules because of its high accuracy and fast analysis speed.[4−6] To make full use of their stable advantage based on the chemical enhancement mechanism (CM), constructing a special charge transfer pathway between the SERS substrates and target molecules is an effective method to further achieve highly selective detection.[7−11] For example, Mahmoud et al.[12] realized the selective SERS detection of 2,4,6-trinitrotoluene (TNT) molecule using the magnetic microsphere PSA/SiO_2/Fe_3O_4/AuNPs (L-MMS) by constructing a hydrogen bond between substrate and target molecule, and the detection limit (LOD) of TNT is lower than 1 pM. Yang et al.[13] constructed a charge transfer pathway by using the "Meisenheimer" complex formed between novel coupling-activated graphene oxide (GO) nanocomposites and TNT, achieving high sensitivity and selectivity for TNT detection (LOD is 60 ppb). In addition, Feng et al.[14] significantly enhanced the charge transfer ability between substrate and target molecules by changing the nitrogen content and lattice type of graphene, achieving LODs of 5×10^{-11}, 1×10^{-8}, and 1×10^{-8} M for rhodamine B (RhB), R_6G, and protoporphyrin IX (PPP), respectively. Yu et al.[15] constructed a local dipole to improve the charge transfer ability on the surface of a graphene oxide substrate, and the enhancement factor (EF) of RhB is 2×10^3. Meng et al.[16] regulated the terminal structure of carbon cloth surfaces to improve the charge transfer ability between substrate and target molecules via surface modification. Obviously, these studies suggest that the construction of special pathways can realize the selective SERS detection of explosives molecules by CM. However, the construction of a specific charge transfer pathway between the carbon substrate and target explosive molecules has not been sufficiently considered in the current research. Especially, the stability and reproducibility of carbon-based materials[17−21] are also their major advantages as SERS

Received: January 22, 2024
Revised: April 7, 2024
Accepted: April 9, 2024
Published: May 9, 2024

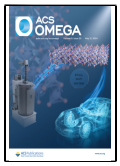

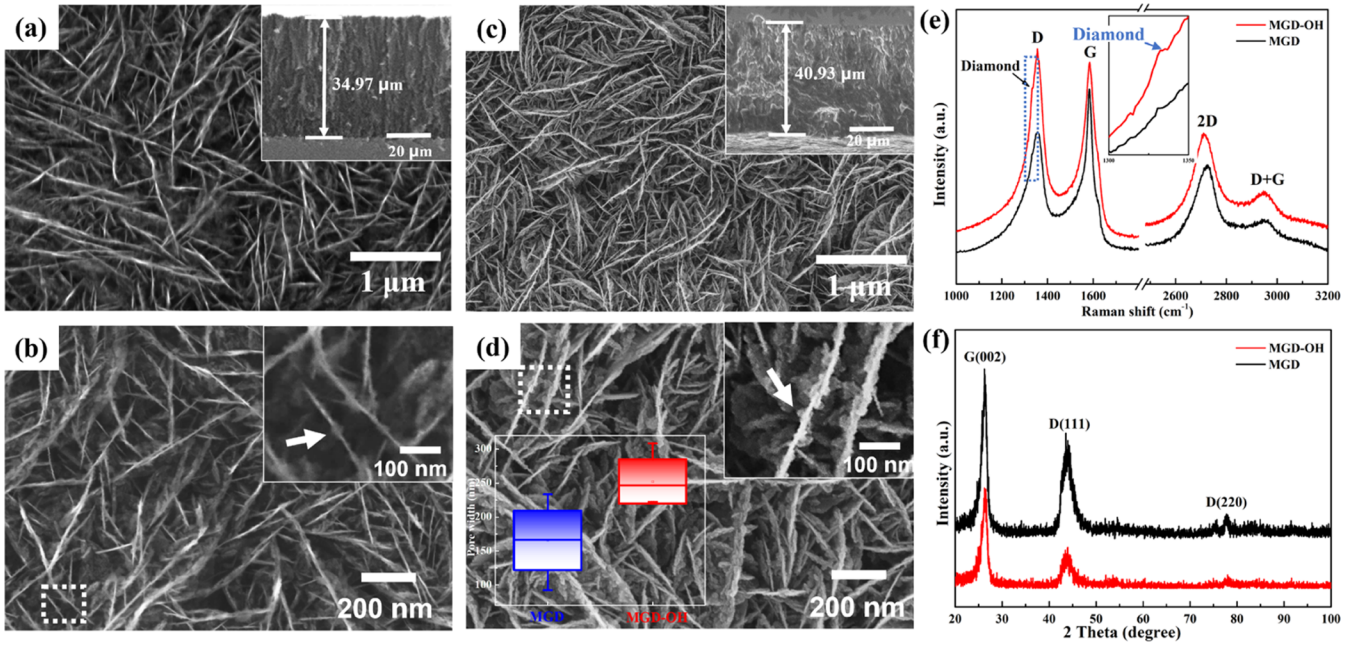

Figure 1. (a) Low-magnification SEM image of MGD thin films (the illustration shows the height of MGD films). (b) High-magnification SEM images of MGD films (the illustration is a high-magnification SEM image of a wire frame enlarged). (c) Low-magnification SEM image of MGD−OH thin films (the illustration shows the height of MGD−OH films). (d) High-magnification SEM images of MGD−OH films (the illustration on the left shows the pore width of MGD and MGD−OH films, and the illustration on the right is a high-magnification SEM image of a wire frame enlarged). (e) Raman spectra of MGD and MGD−OH films. (f) XRD spectra of MGD and MGD−OH films.

substrates. Jiang et al.[22] developed a simple method for preparing an efficient and stable SERS substrate by combining Ag nanoparticles (NPs) and microscale sheeted graphitic carbon nitride (g-C_3N_4), and the EF of crystal violet (CV) is 4.6×10^8. Therefore, surface modification of carbon-based materials with high stability is a good method to achieve high selectivity for explosives.

Herein, on the basis of previous studies of our group proving that the MGD film is an excellent SERS substrate with ultrahigh sensitivity and stability,[23,24] we further modified the surface of MGD films by a two-step wet chemical oxidation of H_2O_2 (30%) and HNO_3 (65%). The experimental results exhibited that hydroxyl (−OH) functional groups were successfully modified on the surface of the MGD film. Compared with unmodified MGD substrates, the MGD−OH substrates demonstrated to have good selectivity for 1,3,5-triamino-2,4,6-trinitrobenzene (TATB) in different concentrations and mixed solutions of explosives (TATB, 2,2-dinitroethene-1,1-diamine (FOX-7), 2,4,6-trinitrotoluene (TNT), and 1,3,5-trinitroperhydro-1,3,5-triazine (RDX)), and the LOD is 10^{-7} M and EF is 814. Meanwhile, the first-principles density functional theory (DFT) calculation is used to further reveal the electron transfer of the characteristic functional group of TATB and the oxygen-containing functional groups of the MGD−OH substrate. This suggests that selective SERS detection of explosive molecules has been realized by constructing a specific charge transfer pathway between the substrate and explosives in a complex environment.

2. EXPERIMENTAL SECTION

2.1. Materials. Si wafers were purchased from Kaihua Silicon Valley Technology Service Co., Ltd. Hydrogen peroxide (H_2O_2, ≥30%), butylamine ($C_4H_{11}N$, ≥99.5%), nitric acid (HNO_3, 65−68%), and acetone (C_3H_6O, ≥99.5%) were purchased from Sinopharm Chemical Reagent Co., Ltd., and used without modification.

Caution! FOX-7 ($C_2H_4N_4O_4$), TATB ($C_6H_6N_6O_6$), TNT ($C_7H_5N_3O_6$), and RDX ($C_3H_6N_6O_6$) compounds have highly explosive characters. They should be used with the best safety protection and with extreme care. Only small quantities (in the *M* range) can be handled during the testing process. All aqueous solutions were prepared with deionized water (18.2 MΩ·cm).

2.2. Synthesis of MGD Films. MGD films were deposited on a Si wafer using a quartz bell in a microwave plasma chemical vapor deposition (MPCVD) reactor. Briefly, *N*-butylamine was used as a sole reactive source and introduced into H_2 plasma through the pressure difference between the vessel used to store *N*-butylamine and the chamber of the MPCVD reactor.

The state of the MGD substrate was changed by wet chemistry to make it easier to form a charge transfer path between the substrate surface and the target explosive molecules. In a two-step wet chemical oxidation of MGD film, the MGD film was oxidized in H_2O_2 for 2 h, then washed with deionized water four times, and dried in the oven. After drying, the MGD film was oxidized in HNO_3 (65−68%) for 2 h and then washed with deionized water six times to obtain the MGD−OH film.

2.3. Characterization. The microstructure of the films was observed using field emission scanning electron microscopy (SEM, Zeiss Sigma 500). Raman spectrum was performed on a commercial system (InVia micro-Raman, Renishaw, U.K.) using a 514.5 nm laser for excitation. The laser power was kept at 5−15 mW, and the Raman emission was collected by a 100× objective via backscattering. Regions of interest were identified from maps for which single spectra were obtained with an acquisition time of 10 s and by integrating once. The

https://doi.org/10.1021/acsomega.4c00749
ACS Omega 2024, 9, 22166−22174

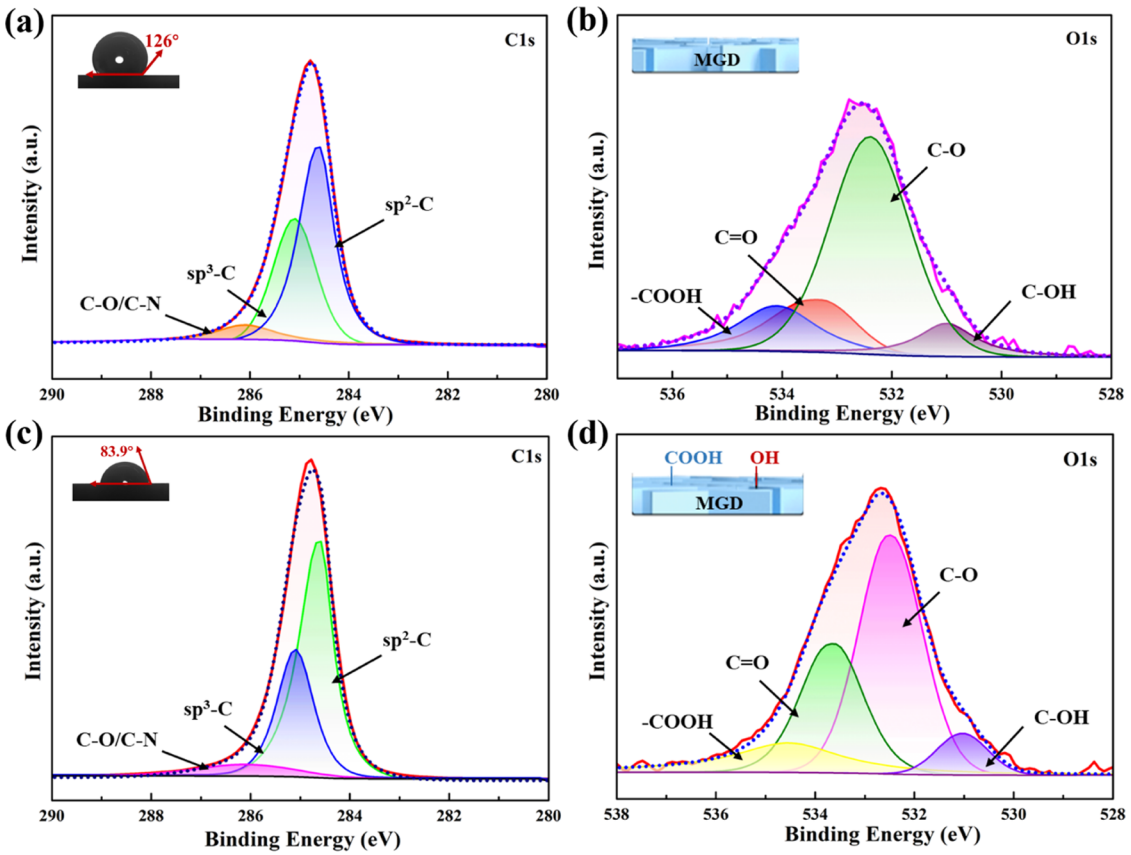

Figure 2. XPS spectra of MGD and MGD−OH films. (a, b) C 1s and O 1s spectra of MGD thin films. (c, d) C 1s and O 1s spectra of MGD−OH thin films.

static water contact angle of the pristine and oxidized MGD films was measured by a K100 instrument. Chemical bonding features of the pristine and MGD−OH films were measured using X-ray photoelectron spectroscopy (XPS, Thermo Scientific K-Alpha, excitation source: Al Kα ray ($h\upsilon$ = 1486.6 eV), beam spot: 400 μm, chamber vacuum better than 5.0 × 10^{-7} mBar, working voltage: 12 kV, filament current: 6 mA; the combined energy standard is C 1s = 284.80 eV).

2.4. SERS Measurements. Before the SERS detection, the explosive molecules (TATB, FOX-7, TNT, RDX) were dissolved in acetone to prepare solutions of different concentrations; 20 μL of explosives with different concentrations were drip-added to Si, MGD, and MGD−OH films. After drying at room temperature for 12 h, SERS detection was conducted under the condition λ = 514.5 nm to evaluate EF and LOD. In the process of measurement, the diameter of the laser spot on the sample is about 1 μm, the integration time of the signal is 10 s (1 time), and the test range is 500−1700 cm^{-1}.

2.5. Theoretical Simulation. The intermolecular interaction between the rGO molecule and TATB was investigated using a density functional theory (DFT) of the ORCA 5.0.3 program package. RIJCOSX was applied to accelerate the calculations. The geometry optimization of these models was performed by using the B3LYP functional with the def2-TZVP(-f) basis set. DFT-D3(BJ) corrections were taken into consideration for each calculation. Also, single-point calculations were performed on the basis of the equilibrium geometries at the B3LYP/def2-TZVP level. All of the structures were fully relaxed until the residual forces on every atom were less than 0.01 eV $Å^{-1}$. To evaluate the SERS enhancement performance between oxygen-containing functional groups and TATB, the vacuum layer was set to larger than 15 Å to avoid interactions between two adjacent slabs.

3. RESULTS AND DISCUSSION

From a low-magnification SEM image (Figure 1a), a large number of vertical nanosheets with a thickness of about 10−15 nm are interlaced with each other, resulting in the formation of a three-dimensional (3D) porous morphology. As shown in the high-magnification SEM image (in the inset of Figure 1b), the small particles attached to both sides of the nanosheet further increase the specific surface area of the MGD film. The cross-sectional SEM in the inset of Figure 1a further displays the vertical growth behavior of the nanosheet, and the height of MGD films is about 34.97 μm for the growth time of 2 h. The structure of the MGD−OH film oxidized by H_2O_2 and HNO_3 is shown in Figure 1c,d. The number of small particles attached to the nanosheet increases obviously, but the height of MGD−OH films increases to 40.93 μm (Figure 1c). It can be observed that there is almost no change in the 3D porous morphology after the H_2O_2 and HNO_3 treatments. The quality of the MGD films by performing Raman spectra is displayed in Figure 1e, where two prominent peaks of the D and G bands are at around 1355 and 1584 cm^{-1},[25] which correspond to disordered sp^3-hybridized carbon featured as defects or impurities and the E_{2g} phonon modes of the sp^2-bonded carbon. A broad and symmetric peak located at 2709 cm^{-1} can be assigned as a second-order (two-dimensional (2D)) process. A weak peak at 2945 cm^{-1} is related to the defects

https://doi.org/10.1021/acsomega.4c00749
ACS Omega 2024, 9, 22166−22174

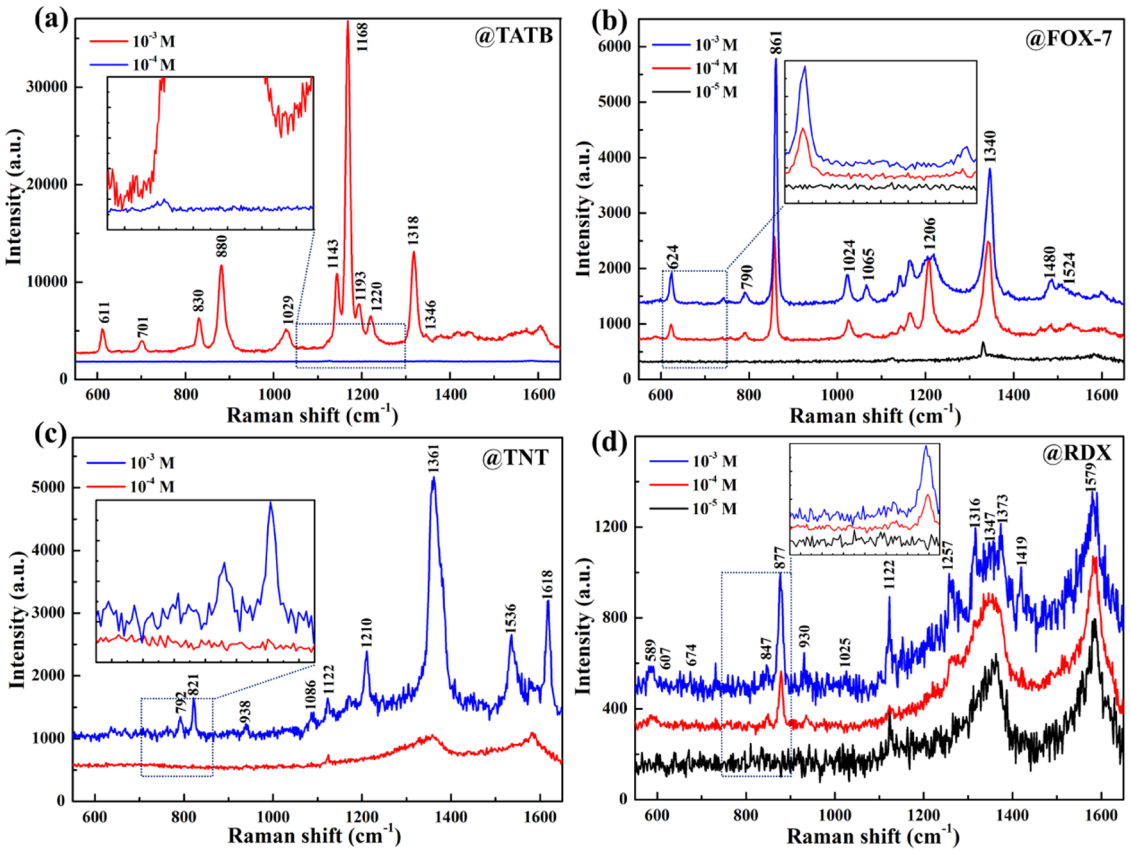

Figure 3. Raman spectra of different explosive molecules detected on the MGD substrate: (a) TATB, (b) FOX- 7, (c) TNT, and (d) RDX.

in the sp^2 sites and a graphene domain edge in the MGD films. The intensity ratio of the 2D to G band is only about 0.50, proving that most of these vertically aligned nanosheets are probably an ultrathin graphene multilayer according to the previous works.[26,27] The weak peak at 1332 cm^{-1} belongs to the diamond peak.[28] Meanwhile, the values of I_D/I_G and I_{2D}/I_G slightly increase to 1.03 and 0.58, respectively, indicating a little increase in the disorder degree after the oxidation treatment. In the grazing incident X-ray diffraction (XRD) pattern (Figure 1f), a sharp peak appears at the 2θ value of about 26.3°, corresponding to the (002) plane of graphite phase, in addition to two board peaks at 43.9 and 78.1° corresponding to the diamond phase.[27,29,30] This result confirms the coexistence of diamond and graphite phases in the MGD films.

The surface of MGD film is hydrophobic, and its contact angle is as large as 126° (in the inset of Figure 2a). Apparently, such a hydrophobic surface would make it difficult for the probe molecules to be adsorbed on the substrate surface. In other words, the 3D porous characteristics of MGD films were not fully utilized. To further achieve the selectivity of the SERS performance, a two-step wet chemical oxidation treatment was performed using a hydrogen peroxide solution as a chemical oxidizing agent. As exhibited in the inset of Figure 2c, the contact angle of MGD−OH films rapidly reduces to 83.9°, confirming the hydrophilic feature. From the XPS spectra, the content of oxygen atoms increases to 5.41% for MGD−OH films, demonstrating that more oxygen-containing functional groups have been grafted on the surface. To obtain the peak positions and relative contributions of chemically shifted components, curve fitting was performed using the Gauss−Lorentz functions.[31] For the MGD films, three subpeaks at 284.8, 285.5, and 286.1 eV can be observed in the C 1s spectrum (Figure 2a), which can be assigned to C-sp^2, C-sp^3, and C−O/C−N, respectively.[22,24] In addition, there are no other peaks in the C 1s spectrum of MGD−OH, but its content changes obviously for thin films (Figure 2c), indicating that the surface state of the thin film changes after oxidation. There are four peaks in the O 1s spectrum (Figure 2b,d) of MGD and MGD−OH thin films, namely, C−OH (531.1 eV), C−O (532.5 eV), C═O (533.6 eV), and −COOH (534.6 eV),[24,32] but the proportion of their oxygen-containing functional groups is different. In other words, the chemical bonding state of the film surface changes after a simple wet chemical treatment with H_2O_2 and HNO_3.

To demonstrate the potential application of MGD films as a SERS substrate, we performed the SERS detection of TATB, FOX-7, TNT, and RDX on the MGD substrate (Figure 3). Figure 3a gives the Raman spectra of TATB molecules with the concentration range from 10^{-3} to 10^{-4} M. Several characteristic peaks at 611, 701, 830, 880, 1029, 1143, 1168, 1193, 1220, 1318, and 1341 cm^{-1},[33] can be clearly observed when the concentration of TATB molecules is not less than 10^{-3} M. The characteristic peak of the substrate at 1352 and 1585 cm^{-1} is not detected, which indicates that the peak of the MGD substrate is completely masked by the signal of the TATB molecule. For comparison, when the concentration of TATB is 1×10^{-4} M, only a weak characteristic peak is observed at 1143 cm^{-1}. It is well-known that the EF value is a very significant parameter to evaluate a SERS substrate, which can be calculated by[34]

https://doi.org/10.1021/acsomega.4c00749
ACS Omega 2024, 9, 22166−22174

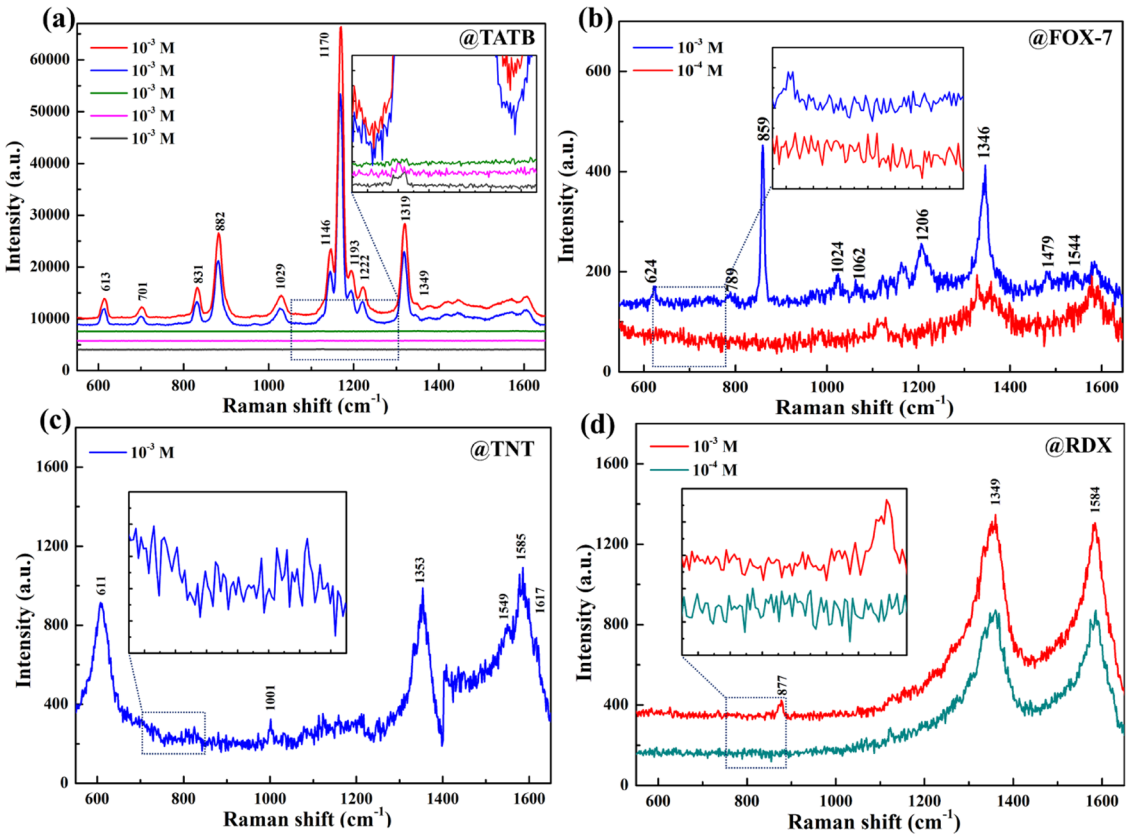

Figure 4. Raman spectra of different explosive molecules detected on the MGD−OH substrate: (a) TATB, (b) FOX- 7, (c) TNT, and (d) RDX.

$$\mathrm{EF} = \frac{I_{\mathrm{SERS}}/C_{\mathrm{SERS}}}{I_0/C_0} \quad (1)$$

where I_{SERS} and I_0 represent the peak intensities of the SERS spectra and the normal Raman spectra, respectively. C_{SERS} and C_0 are the concentrations of molecules on the SERS and normal substrate, respectively. Using the peak at 1169 cm^{-1} (C-NO_2 stretching + NO_2 deformation + C-NH_2 stretching + H−N−H shearing) as a criterion, we can further estimate that the EF value of TATB molecules on the MGD substrate is as high as 565. Figure 3b is the Raman spectra of FOX-7 molecules with the concentration range from 10^{-3} to 10^{-5} M. Several characteristic peaks at 624, 790, 861, 1024, 1065, 1206, 1340, 1480, and 1524 cm^{-1},[35] can be clearly seen when the concentration of TATB molecules is 10^{-3} M. Even when the concentration was as low as 10^{-5} M, a weak characteristic peak could be detected at 1340 cm^{-1}. Using the peak at 856 cm^{-1} (N−O + NH common vibration mode) as a criterion, we can further estimate that the EF value of FOX-7 molecules on the MGD substrate is 3.2. Figure 3c displays the Raman spectra of TNT molecules with the concentration range from 10^{-3} to 10^{-4} M. Several characteristic peaks at 792, 821, 1210, 1361, 1536, and 1618 cm^{-1},[36] can be clearly observed when the concentration of TNT molecules is 10^{-3} M. Using the peak at 1208 cm^{-1} ($-CH_3$ vibration) as a criterion, we can further estimate that the EF value of TNT molecules on the MGD substrate is 2.3. Figure 3d demonstrates the Raman spectra of RDX molecules with the concentration range from 10^{-3} to 10^{-5} M. Several characteristic peaks at 589, 607, 674, 847, 882, 930, 1025, 1257, 1316, and 1419 cm^{-1},[37] can be clearly seen when the concentration of RDX molecules 10^{-4} M. Using the peak at 877 cm^{-1} (ring bending and O−N−O tension) as a criterion, we can further estimate that the EF value of RDX molecules on the MGD substrate is 3.8. The results exhibited that MGD films have a certain enhancement ability for four kinds of explosives, especially for TATB molecules, which indicates that MGD films have a certain application potential in the SERS detection of explosives.

Similarly, using the MGD−OH films as a SERS substrate, we further discovered that the performances could be remarkably improved. For the TATB molecules, the LOD value is as low as 10^{-7} M (Figure 4a) and the EF value increases to 814. For the FOX-7, TNT, and RDX molecules (Figure 4b−d), a part of the Raman signals can gradually disappear and/or be submerged due to strong characteristic Raman peaks (D and G bands) of the MGD−OH substrate. Using the formula (eq 1), it is calculated that the EF, FOX-7, and TNT are 0.23 and 0.3, respectively, almost only the base signal. In other words, the MGD−OH substrate has excellent enhancement and selectivity to TATB, and the Raman signals of FOX-7, TNT, and RDX are suppressed.

Next, the anti-interference, uniformity, and stability SERS performance of the MGD−OH film for the detection of the TATB explosive were further evaluated. Four solutions were prepared with TATB, FOX-7, TNT, and RDX at the same concentrations (10^{-3} M) by mixing the analyte solutions in equal volumes, as shown in Figure 5a, several characteristic peaks at 616, 703, 833, 883, 1030, 1146, 1170, 1196, 1221, 1320, and 1348 can be clearly observed in the mixture of TATB, TNT, FOX-7, and RDX. The results show that no matter in which mixed solution, the intensity of the characteristic peak will be affected to a certain extent, but the characteristic peak of TATB is not affected by other explosives, indicating that the MGD−OH film has a certain

https://doi.org/10.1021/acsomega.4c00749
ACS Omega 2024, 9, 22166−22174

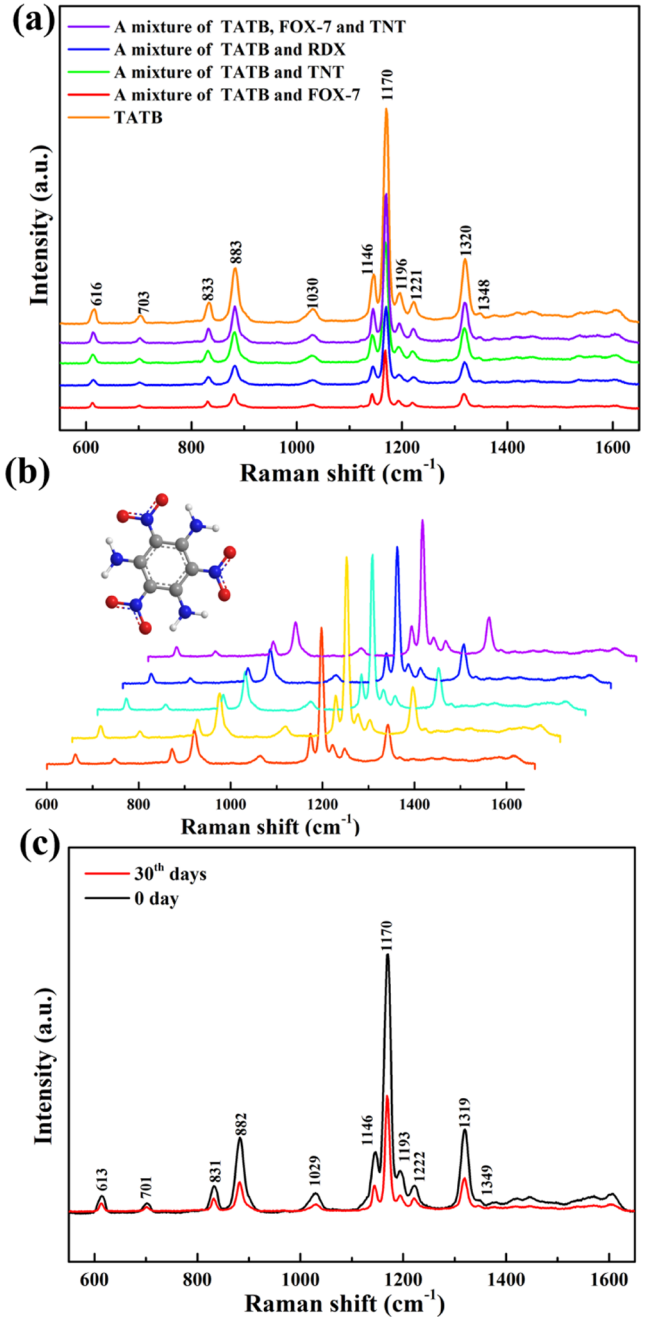

Figure 5. SERS of TATB molecules on the MGD−OH substrate. (a) Raman spectra of TATB molecules in different mixed solutions detected by the MGD−OH substrate. (b) Raman spectra of TATB molecules with a concentration of 10^{-3} M, randomly collected from five positions in the same MGD−OH substrate. (c) Raman spectra of TATB molecules (the solution on 10^{-3} M) measured on the 0th day and 30th day, respectively.

degree of anti-interference in the detection of TATB. As shown in Figure 5b, almost the same Raman spectra can be observed, indicating good uniformity. From a quantitative point of view, the relative standard deviation (RSD) of Raman intensity corresponding to the peak at 1170 cm^{-1} is about 12.7%. In addition, the stability of the MGD−OH substrate was evaluated by using the variation of Raman intensity of the peak at 1170 cm^{-1}. In addition, the SERS stability of the MGD−OH film for the detection of the TATB explosive after exposure to the air for 30 days is shown in Figure 5c, and the Raman intensity of peak at 1170 cm^{-1} decreases about 27.6% for the MGD−OH films, also demonstrating good long-term stability. All of the above observations manifest that MGD−OH films are an effective SERS substrate for the TATB probe molecule with low LOD, large EF, high uniformity, and excellent stability. Table 1 summarizes the typical SERS performances of other substrates reported in recent years.[12,13,38−51] Compared with other substrates used for the detection of explosives, MGD and the O-MGD films show better selectivity for TATB.

Coincidentally, the SERS detection performance of MGD−OH films was also better than that of MGD films for the real TATB molecules. To further understand the SERS mechanism of the characteristically functional group of TATB and the oxygen-containing functional groups (−OH, −COOH) of the MGD−OH substrate, DFT calculations were carried out to achieve further insight into the adsorption energy and electron transfer performance.[52] The surface of the oxidized MGD−OH substrate is rich in oxygen-containing groups such as −OH and −COOH. Figure 6a shows the electrostatic potential diagram of the interaction between TATB-NO_2 and the MGD−OH surface −OH and −COOH groups. The electrostatic potential is positive, indicating that this area is easier to gain electrons (TATB) and has electrophilicity. On the contrary, the electrostatic potential is negative, indicating that this region is more likely to give electrons (−OH, −COOH) and has nucleophilic properties. Therefore, it is easy to form a charge transfer path to enhance the Raman signal. The theoretical simulation results demonstrate that the interaction between −OH and $-NO_2$, −OH and $-NH_2$, and −COOH and $-NO_2$ is −5.607, −7.514, and −9.882 kcal·mol^{-1}, respectively. The more negative the adsorption energy, the stronger the interaction between groups. In other words, the hydrogen bond strength between −COOH and $-NO_2$ is stronger than that between −OH and $-NO_2$ and that between −OH and $-NH_2$. Next, we compare the TATB electron transfer properties of different functional groups on the surface of graphene oxide to obtain the kinetic point of view of surface-mediated bond chemistry. The calculation results of TATB display that when −OH is close to $-NH_2$ (Figure 6b), the N atoms of TATB lose 0.004, 0.002, and −0.008 e^-, and the H atoms of TATB gain 0.003 and −0.018 e^-, the O atoms of TATB gain 0.007, 0.006, 0.005, and −0.018 e^-, the benzene ring of TATB gains 0.028 e^-, and the O atoms of −OH lose 0.028 e^-. The calculation results of TATB show that when −OH is close to $-NO_2$ (Figure 6c), the N atoms of TATB lose 0.004, −0.057, and 0.016 e^-, the H atoms of TATB gain 0.002 e^-, the O atoms of TATB lose 0.057 and 0.016 e^-, the benzene ring of TATB gain 0.018 e^-, and the H atoms of −OH gain 0.018 e^-. The calculation results of TATB indicate that when −COOH is close to $-NO_2$ (Figure 6d), the N atoms of TATB gain 0.024, −0.038, and 0.012 e^-, the H atoms of TATB lose 0.001, −0.010, 0.002, and 0.0002 e^-, the O atoms of TATB lose 0.056 and 0.009 e^-, the benzene ring of TATB loses 0.011 e^-, and the H atoms of −COOH gain 0.011 e^-. Obviously, the charge transfer between the $-NH_2$ functional group and −OH, $-NO_2$ functional group, and −COOH in TATB is more likely. This result corresponds to the detection of TATB on the MGD−OH substrate. Hydrogen bonds are formed between −OH and −COOH and TATB molecules, which promote charge transfer between the MGD−OH substrate and TATB molecule after laser excitation.

https://doi.org/10.1021/acsomega.4c00749
ACS Omega 2024, 9, 22166−22174

Table 1. Comparison of the EF, LOD, Stability, and Selectivity of MGD and O-MGD Films for SERS Detection in Explosives with Different Substrates

substrate	probe	EF	LOD	stability	selectivity	references
L-MMS	TNT		<1 pM		TNT	12
coupling-activated GO nanocomposites	TNT		60 ppb		TNT	13
Au-AgNPs/glass	TNT, RDX		pg levels			38
AgNPs/hydrophilic photonic crystal biosilica	TNT		10^{-10} M			39
AuNPs/TiO_2 NR	TNT	4×10^6	10^{-7} M			40
AuNPs and nanostructures	2,4,6-trinitrophenol (PA)		10 μM			41
Ag−Cu alloy NPs	PA	2.8×10^4	5 μM			42
	AN	3.3×10^4	5 μM			
Ag−AuNPs/NSs	FOX-7	10^8	5 μM			43
Ag@AuNPs	PA	10^4	10^{-6} M			44
CuNPs with rough edges	5-amino-3-nitro-1,2,4-triazole (ANTA), FOX-7		2×10^{-4} M			45
Ag sinusoidal nanograting	TNT	10^4	10^{-5} M			46
AuTNPs/glass	TNT, RDX, PETN	6×10^6	10^{-6} M			47
hydrophobic Ag nanopillars	PA		20 ppt			48
Au nanocage/GO	TNT, RDX	10^{11}				49
AgNCs/borosilicate slides	RDX	10^{11}				50
	TNT	10^{11}				
Ag/ZnO film	ANTA	10^7				51
	FOX-7	10^7				
	CL-20	10^4				
MGD film	TATB	565	10^{-4} M	30 days		this work
O-MGD film		814	10^{-7} M		TATB	

Abbreviations: **TNT:** 2,4,6-trinitrotoluene; **RDX:** cyclotrimethylenetrinitramine; **PA:** 2,4,6-trinitrophenol; **FOX-7:** 1-diamino-2,2-dinitroethene; **ANTA:** 5-amino-3-nitro-1,2,4-triazole; **PETN:** penthrite(pentaerythritol tetranitrate); **CL-20:** 2,4,6,8,10,12-hexanitro-2,4,6,8,10,12-hexaazaiso-wurtzitane; **GO:** graphene oxide.

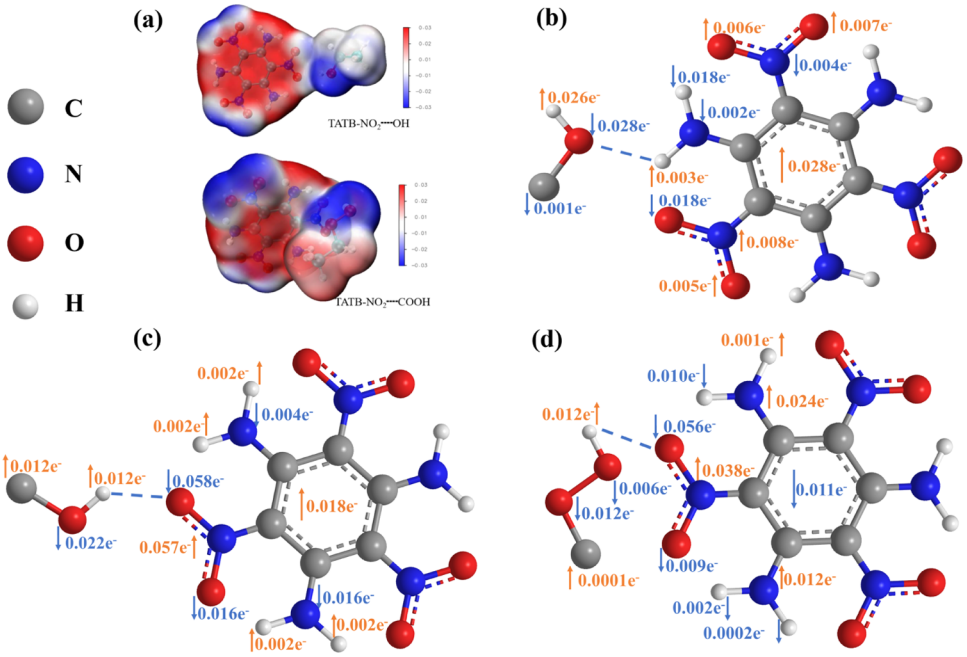

Figure 6. (a) Electrostatic potential diagram of the interaction between TATB-NO_2 and −OH and −COOH groups on the surface of MGD−OH materials. (b) Charge transfer between $-NH_2$ of TATB and −OH of the substrate. (c) Charge transfer between $-NO_2$ of TATB and −OH of the substrate. (d) Charge transfer between $-NO_2$ of TATB and −COOH of the substrate.

4. CONCLUSIONS

In summary, the −OH terminal group was successfully modified on the surface of MGD. The SERS results displayed that the MGD−OH substrate has good selectivity for TATB in different concentrations and mixed solutions of TATB, FOX-7, TNT, and RDX explosives (LOD is 10^{-7} M and EF is 814), good uniformity (RDS is 12.7%), and good stability (the characteristic peak signal only decreases by 27.6% after 30 days). In addition, the DFT calculation revealed that the selectivity of SERS performance is attributed to the construction of the charge transfer path between the $-NO_2$

https://doi.org/10.1021/acsomega.4c00749
ACS Omega 2024, 9, 22166−22174

functional group of TATB and the −OH functional group of MGD−OH. This study provides great potential to bring a new way for the recognition of residual explosives in soldiers' bodies or in the natural environment.

AUTHOR INFORMATION

Corresponding Authors

Huiqiang Liu − *School of Materials & Chemistry, Southwest University of Science & Technology, Mianyang 621010, China*; orcid.org/0000-0002-4477-891X; Email: liuhuiqiang@swust.edu.cn

Ying Xiong − *State Key Laboratory for Environment-Friendly Energy Materials and School of Materials & Chemistry, Southwest University of Science & Technology, Mianyang 621010, China*; Email: xiongying@swust.edu.cn

Authors

Lin Jiang − *State Key Laboratory for Environment-Friendly Energy Materials and School of Materials & Chemistry, Southwest University of Science & Technology, Mianyang 621010, China*

Bing Wang − *School of Materials & Chemistry, Southwest University of Science & Technology, Mianyang 621010, China*

Wen Zhang − *State Key Laboratory for Environment-Friendly Energy Materials, Southwest University of Science & Technology, Mianyang 621010, China*

Jian Wang − *Joint Laboratory for Extreme Conditions Matter Properties, School of Mathematics and Physics, Southwest University of Science and Technology, Mianyang 621010 Sichuan, China*

Complete contact information is available at: https://pubs.acs.org/10.1021/acsomega.4c00749

Notes

The authors declare no competing financial interest.

ACKNOWLEDGMENTS

This work was supported by the National Natural Science Foundation of China (Grant No. 62374140), the Natural Science Foundation of Sichuan Province (Project Nos. 2022NSFSC0523 and 21zs2232), the Sichuan Science and Technology Program (Grant No. 2023NSFSC1990), the Natural Science Foundation of Xi'an Modern Chemistry Research Institute (Grant No. 21zh0175), and the Natural Science Foundation of Southwest University of Science and Technology (Project No. 20zx7103)

REFERENCES

(1) Chen, T. F.; Lu, S. H.; Wang, A. J.; Zheng, D.; Wu, Z. L.; Wang, Y. S. Detection of explosives by surface enhanced Raman scattering using substrate with a monolayer of ordered Au nanoparticles. *Appl. Surf. Sci.* **2014**, *317*, 940−945.

(2) Weinberger, S. Airport security: Intent to deceive? *Nature* **2010**, *465*, 412−415.

(3) Chatterjee, S.; Deb, U.; Datta, S.; Walther, C.; Gupta, D. K. Common explosives (TNT, RDX, HMX) and their fate in the environment: Emphasizing bioremediation. *Chemosphere* **2017**, *184*, 438−451.

(4) Tan, Y. H.; Yang, K.; Zhang, X. F.; Zhou, Z. Y.; Xu, Y. T.; Xie, A. T.; Xue, C. G. Stretchable and Flexible Micro-Nano Substrates for SERS Detection of Organic Dyes. *ACS Omega* **2023**, *8*, 14541−14548.

(5) Jiang, J. Z. Improving the surface-enhanced Raman scattering activity of carbon nitride by two-step calcining. *RSC Adv.* **2016**, *6*, 47368−47372.

(6) Jiang, J. Z.; Zou, J.; Wee, A. T. S.; Zhang, W. J. Use of Single-Layer g-C3N4/Ag Hybrids for Surface-Enhanced Raman Scattering (SERS). *Sci. Rep.* **2016**, *6* (1−10), No. 34599.

(7) Wu, J. J.; Zhang, L.; Huang, F.; Ji, X. X.; Dai, H. Q.; Wu, W. B. Surface enhanced Raman scattering substrate for the detection of explosives: construction strategy and dimensional effect. *J. Hazard. Mater.* **2020**, *387*, No. 121714.

(8) Yang, B.; Jin, S.; Guo, S.; Park, Y.; Chen, L.; Zhao, B.; Jung, Y. M. Recent development of SERS technology: semiconductor-based study. *ACS Omega* **2019**, *4*, 20101−20108.

(9) Deng, F. X.; Jiang, J. Z.; Sirés, I. State-of-the-art review and bibliometric analysis on electro-Fenton process. *Carbon Lett.* **2023**, *33*, 17−34.

(10) Li, F. Y.; Anjarsari, Y.; Wang, J. M.; Azzahiidah, R.; Jiang, J. Z.; Zou, J.; Xiang, K.; Ma, H. J.; Arramel. Modulation of the lattice structure of 2D carbon-based materials for improving photo/electric properties. *Carbon Lett.* **2023**, *33*, 1321−1331.

(11) Wang, J. M.; Qin, Q.; Li, F. Y.; Anjarsari, Y.; Sun, W.; Azzahiidah, R.; Zou, J.; Xiang, K.; Ma, H. J.; Jiang, J. Z.; Arramel. Recent advances of MXenes Mo_2C-based materials for efficient photocatalytic hydrogen evolution reaction. *Carbon Lett.* **2023**, *33*, 1381−1394.

(12) Mahmoud, K. A.; Zourob, M. Fe_3O_4/Au nanoparticles/lignin modified microspheres as effectual surface enhanced Raman scattering (SERS) substrates for highly selective and sensitive detection of 2,4,6-trinitrotoluene (TNT). *Analyst* **2013**, *138*, 2712−2719.

(13) Yang, J.; Gao, W. Y.; Wang, T. R.; Zhu, C. S.; Dong, P. T.; Wu, X. Z. A novel coupling-activated GO nanocomposites based on surface acoustic wave for assessing capture molecules and detection of explosive gases. *Sens. Actuators, B* **2022**, *372*, No. 132665.

(14) Feng, S.; Santos, M. C.; Carvalho, B. R.; Lv, R.; Li, Q.; Fujisawa, K.; Elías, A. L.; Lei, Y.; Perea-López, N.; Endo, M.; Pan, M.; Pimenta, M. A.; Terrones, M. Ultrasensitive molecular sensor using N-doped graphene through enhanced Raman scattering. *Sci. Adv.* **2016**, *2*, No. 1600322.

(15) Yu, X. X.; Lin, K.; Qiu, K. Q.; Cai, H. B.; Li, X. J.; Liu, J. Y.; Pan, N.; Fu, S. J.; Luo, Y.; Wang, X. P. Increased chemical enhancement of Raman spectra for molecules adsorbed on fluorinated reduced graphene oxide. *Carbon* **2012**, *50*, 4512−4517.

(16) Meng, S. J.; Liang, J. X.; Jia, W. M.; Zhang, P.; Su, Q.; Wang, C. J.; An, L. L.; Chen, L. H.; Wang, Y. B. Metal-free and flexible surface-enhanced Raman scattering substrate based on oxidized carbon cloth. *Carbon* **2022**, *189*, 152.

(17) Jiang, J. Z. Novel Applications of Micro/Nanostructured Volcanic Ash for Water Purification and Surface-Enhanced Raman Spectroscopy. *Anal. Lett.* **2016**, *49*, 2793−2806.

(18) Zou, J.; Wu, J.; Wang, Y. Z.; Deng, F. X.; Jiang, J. Z.; Zang, Y. Z.; Liu, S.; Li, N.; Zhang, H.; Yu, J. G.; Zhai, T. Y.; N Alshareef, H. Additive-mediated intercalation and surface modification of Mxenes. *Chem. Soc. Rev.* **2022**, *51*, 2972−2990.

(19) Park, S. Y.; Lee, S. Y. Analysis of the amorphous SiInZnO/Ag/amorphous SiInZnO multilayer structure as a next-generation transparent electrode using essential macleod program simulation. *Carbon Lett.* **2023**, *33*, 1231−1239.

(20) Wang, H.; Wang, H. T.; Yang, J. J.; Maulida, P. Y. D.; Zou, J.; Arramel; Wu, C.; Jiang, J. Z. Black phosphorus nanosheets-based effective electrochemical sensor for uric acid detection. *Carbon Lett.* **2023**, *33*, 2161−2169.

(21) Jiang, J. Z.; Ou-Yang, L.; Zhu, L. H.; Zou, J.; Tang, H. Q. Novel one-pot fabrication of lab-on-a-bubble@Ag substrate without coupling-agent for surface enhanced Raman scattering. *Sci. Rep.* **2014**, *4*, No. 3942.

(22) Jiang, J. Z.; Zhu, L. H.; Zou, J.; Ou-Yang, L.; Zheng, A. M.; Tang, H. Q. Micro/nano-structured graphitic carbon nitride-Ag nanoparticle hybrids as surface-enhanced Raman scattering substrates with much improved long-term stability. *Carbon* **2015**, *87*, 193−205.

(23) Li, H. N.; Yang, B.; Yu, B.; Huang, N.; Liu, L. S.; Lu, J. Q.; Jiang, X. Graphene-coated Si nanowires as substrates for surface-enhanced Raman scattering. *Appl. Surf. Sci.* **2021**, *541*, No. 148486.
(24) Qu, H. X.; Liu, H. Q.; Wang, B.; Jiang, L.; Zhang, P.; Liu, G. Q.; Xiong, Y. A three dimensional porous diamond-multilayer graphene nanohybrid film for surface-enhanced Raman spectroscopy. *Diamond Relat. Mater.* **2022**, *121*, No. 108737.
(25) Dresselhaus, M. S.; Jorio, A.; Saito, R. Characterizing Graphene, Graphite, and Carbon nanotubes by Raman spectroscopy. *Annu. Rev. Condens. Matter Phys.* **2010**, *1*, 89−108.
(26) Xu, W. G.; Mao, N. N.; Zhang, J. Graphene: a platform for surface-enhanced Raman spectroscopy. *Small* **2013**, *9*, 1206−1224.
(27) Li, H. N.; Xiong, Y.; Wang, B.; Yang, B.; Huang, N.; Liu, Y.; Wen, J. W. Microstructural modification of diamond-graphite nanohybrid films via adjusting deposition temperatures for enhanced electron field emission. *Diamond Relat. Mater.* **2018**, *87*, 228−332.
(28) Prawer, S.; Nemanich, R. J. Raman spectroscopy of diamond and doped diamond. *Philos. Trans. R. Soc., A* **2004**, *362*, 2537−2565.
(29) Zhai, Z. F.; Huang, N.; Yang, B. P.; Wang, C.; Liu, L. S.; Qiu, J. H.; Shi, D.; Yuan, Z. Y.; Lu, Z. G.; Song, H. Z.; Zhou, M. Q.; Chen, B.; Jiang, X. Insight into the effect of the core-shell microstructure on the electrochemical properties of undoped 3D-networked conductive diamond/graphite. *J. Phys. Chem. C* **2019**, *123*, 6018−6029.
(30) Zhang, G. R.; Liu, H. Q.; Xiao, Y. X.; Wang, B.; Wang, J.; Zhang, W.; Xiong, Y. Orientated growth the 3D diamond/graphene hybrid arrays and the application in thermal interface materials. *Funct. Diamond* **2022**, *2*, 263−270.
(31) Xu, L. L.; Zhan, H.; Tian, Y.; Jiao, A. X.; Li, S.; Tan, Y.; Chen, M.; Chen, F. Modified photochemical strategy to support highly-purity, dense and monodisperse Au nanospheres on graphene oxide for optimizing SERS detection. *Talanta* **2020**, *209*, No. 120535.
(32) Rabchinskii, M. K.; Saveliev, S. D.; Stolyarova, D. Y.; Brzhezinskaya, M.; Kirilenko, D. A.; Baidakova, M. V.; Ryzhkov, S. A.; Shnitov, V. V.; Sysoev, V. V.; Brunkov, P. N. Modulating nitrogen species via n-doping and post annealing of graphene derivatives: XPS and XAS examination. *Carbon* **2021**, *182*, 593−604.
(33) Liu, H.; Zhao, J. J.; Ji, G. F.; Wei, D. Q.; Gong, Z. Z. Vibrational properties of molecule and crystal of TATB: A comparative density fictional study. *Phys. Lett. A* **2006**, *358*, 63−69.
(34) Le Ru, E. C.; Blackie, E.; Meyer, M.; Etchegoin, P. G. Surface Enhanced Raman Scattering Enhancement Factors: A Comprehensive Study. *J. Phys. Chem. C* **2007**, *111*, 13794−13803.
(35) He, X.; Liu, Y.; Liu, Y.; Cui, S.; Liu, W.; Li, Z. B. Controllable fabrication of Ag-NP-decorated porous ZnO nanosheet arrays with superhydrophobic for high performance SERS detection of explosives. *CrystEngComm* **2020**, *22*, 776−785.
(36) Heleg-Shabtai, V.; Zaltsman, A.; Sharon, M.; Sharabi, H.; Nir, I.; Marder, D.; Cohen, G.; Rona, I.; Pevzner, A. Explosive vapour/particles detection using SERS substrates and a hand-held Raman detector. *RSC Adv.* **2021**, *11*, 26029.
(37) Dreger, Z. A.; Gupta, Y. M. High pressure Raman spectroscopy of single crystals of hexahydro-1, 3, 5-trinitro-1, 3, 5-triazine (RDX). *J. Phys. Chem. B* **2007**, *111*, 3893−3903.
(38) Guenther, D.; Dowgiallo, A. M.; Branham, A. Trace-level detection of explosives using sputtered SERS substrates. *Spectroscopy* **2017**, *32*, 8−17.
(39) Kong, X. M.; Xi, Y. T.; Duff, P. L.; Chong, X. Y.; Li, E.; Ren, F. H.; Rorrer, G. L.; Wang, A. X. Detecting explosive molecules from nanoliter solution: a new paradigm of SERS sensing on hydrophilic photonic crystal biosilica. *Biosens. Bioelectron.* **2017**, *88*, 63−70.
(40) Samransuksamer, B.; Horprathum, M.; Jutarosaga, T.; Kopwitthaya, A.; Limwichean, S.; Nuntawong, N.; Chananonnawathorn, C.; Patthanasettakul, V.; Muthitamongkol, P.; Treetong, A.; Klamchuen, A.; Leelapojanaporn, A.; Thanachayanont, C.; Eiamchai, P. Facile method for decorations of Au nanoparticles on TiO_2 nanorod arrays toward high-performance recyclable SERS substrates. *Sens. Actuators, B* **2018**, *277*, 102−113.
(41) Byram, C.; Morama, S. S. B.; Soma, V. R. SERS based detection of multiple analytes from dye/explosive mixtures using picosecond laser fabricated gold nanoparticles and nanostructures. *Analyst* **2019**, *144*, 2327−2336.
(42) Satya Bharati, M. S.; Chandu, B.; Rao, S. V. Explosives sensing using Ag-Cu alloy nanoparticles synthesized by femtosecond laser ablation and irradiation. *RSC Adv.* **2019**, *9*, 1517−1525.
(43) Podagatlapalli, G. K.; Hamad, S.; Rao, S. V. Trace-level detection of secondary ex-plosives using hybrid silver-gold nanoparticles and nanostructures achieved withfemtosecond laser ablation. *J. Phys. Chem. C* **2015**, *119*, 16972−16983.
(44) Sree Satya Bharati, M.; Byram, C.; Soma, V. R. Femtosecond laser fabricated Ag@Au and Cu@Au alloy nanoparticles for surface enhanced raman spectroscopy based trace explosives detection. *Front. Phys.* **2018**, *6*, 28 DOI: 10.3389/fphy.2018.00028.
(45) Hamad, S.; Podagatlapalli, G. K.; Mohiddon, M. A.; Rao, S. V. Surface enhanced fluorescence from corroles and SERS studies of explosives using copper nanostructures. *Chem. Phys. Lett.* **2015**, *621*, 171−176.
(46) Xiao, C.; Chen, Z. B.; Qin, M. Z.; Zhang, D. X.; Fan, L. Composite sinusoidal nanograting with long-range SERS effect for label-free TNT detection. *Photonic Sens.* **2018**, *8*, 278−288.
(47) Liyanage, T.; Rael, A.; Shaffer, S.; Zaidi, S.; Goodpaster, J. V.; Sardar, R. Fabricationof a self-assembled and flexible SERS nano-sensor for explosive detection at parts-per-quadrillion levels from fingerprints. *Analyst* **2018**, *143*, 2012−2022.
(48) Hakonen, A.; Wang, F. C.; Andersson, P. O.; Wingfors, H.; Rindzevicius, T.; Schmidt, M. S.; Soma, V. R.; Xu, S. C.; Li, Y. Q.; Boisen, A.; Wu, H. A. Hand-held femtogram detection of hazardous picric acid with hydrophobic ag nanopillar sers substrates and mechanism of elasto-capillarity. *ACS Sens.* **2017**, *2*, 198−202.
(49) Kanchanapally, R.; Sinha, S. S.; Fan, Z.; Dubey, M.; Zakar, E.; Ray, P. C. Graphene oxide-gold nanocage hybrid platform for trace level identification of nitro explosives using a raman fingerprint. *J. Phys. Chem. C* **2014**, *118*, 7070−7075.
(50) Ben-Jaber, S.; Peveler, W. J.; Quesada-Cabrera, R.; Sol, C. W. O.; Papakonstantinou, I.; Parkin, I. P. Sensitive and specific detection of explosives in solution and vapour by surface-enhanced Raman spectroscopy on silver nanocubes. *Nanoscale* **2017**, *9*, 16459−16466.
(51) Shaik, U. P.; Hamad, S.; Ahamad Mohiddon, M.; Soma, V. R.; Ghanashyam Krishna, M. Morphologically manipulated Ag/ZnO nanostructures as surface enhancedRaman scattering probes for explosives detection. *J. Appl. Phys.* **2016**, *119*, No. 093103.
(52) Lu, T.; Chen, F. W. Multiwfn: A multifunctional wavefunction analyzer. *J. Comput. Chem.* **2012**, *33*, 580−592.

https://doi.org/10.1021/acsomega.4c00749
ACS Omega 2024, 9, 22166−22174